Solar Energy Materials and Solar Cells 200 (2019) 109990

Contents lists available at ScienceDirect

Solar Energy Materials and Solar Cells

journal homepage: www.elsevier.com/locate/solmat

Degradation and regeneration of radiation-induced defects in silicon: A study of vacancy-hydrogen interactions

Muhammad U. Khan[a,*], Daniel Chen[a], Saman Jafari[a], Takeshi Ohshima[b], Hiroshi Abe[b], Ziv Hameiri[a], Chee Mun Chong[a], Malcolm Abbott[a]

[a] School of Photovoltaic and Renewable Energy Engineering, UNSW, Sydney, NSW, 2052, Australia
[b] National Institutes for Quantum and Radiological Science and Technology, Takasaki, Gunma, 370-1292, Japan

ARTICLE INFO

Keywords:
LeTID
Hydrogen
Electron radiation
Vacancy
Silicon

ABSTRACT

Silicon lattice vacancies exist in all silicon wafers, will increase in concentration due to high temperature processing, can form recombination active defects and have been proposed as a possible candidate for LeTID. Despite this, there have been relatively few studies in the solar field dedicated to investigating vacancies, their recombination properties or their interaction with hydrogen. In this work, we use high energy electron radiation to create large numbers of vacancies in silicon and study the lifetime response to subsequent thermal processes in the presence or absence of bulk hydrogen. The radiation results in the formation of radiation-induced defects which we interpret as being related to the creation of vacancies in the silicon bulk. Modelling of injection dependent minority carrier lifetime finds that the defects formed via this radiation process have different Shockley-Read-Hall properties to LeTID and are as such, unlikely to be related. Furthermore, this defect can be removed during low temperature annealing but only if hydrogen is present in the bulk of the silicon wafers. This is in contrast to samples with no bulk hydrogen which do not recover during low temperature annealing. The study thus finds no evidence for any link between LeTID and vacancies in silicon, but it does demonstrate the ability of hydrogen to repair radiation damage.

1. Introduction

Silicon micro-defects, vacancies and self-interstitials are fundamental defects which can be produced during crystallization [1], during high-temperature thermal processes [2,3] or as a result of direct lattice damage (e.g. from high energy radiation) [4,5]. Once created, vacancies and self-interstitials move rapidly through the silicon lattice and may act individually as recombination centres or may pair with other impurities (including themselves) to form a variety of recombination active defects [6–9]. Lattice defects like grain boundaries, dislocations, external surfaces, or voids can act as a source or sink for vacancies which may lead to a variety of complex kinetic behavior [10]. Recently, it has been proposed that the role of fundamental point defects in the degradation of solar cells should be examined in more detail [7,11–14]. In this work, we use electron radiation to create vacancy-related defects and further investigate such defects in the context of solar cell degradation.

Degradation in the performance of terrestrial solar cells during operation (particularly when exposed to carrier injection) reduces the annual yield of photovoltaic systems and has several root causes. One major loss mechanism is related to degradation in the carrier lifetime within the bulk of the absorber material due to the formation of metastable defects. Several such defects have been identified and studied, although of concern to the industry at present is the so-called light and elevated temperature-induced degradation (LeTID) [15]. The root cause of which remains a topic of active investigation [15–17]. The recombination active boron and oxygen (BO) complex that forms due to carrier injection in Czochralski (Cz) silicon [18] cannot explain LeTID as BO has different Shockley-Read-Hall (SRH) properties [15] and has been observed in Ga doped silicon [19] and n-type silicon [20] where there is insignificant amounts of boron. Many researchers have suggested that hydrogen plays a key role in the formation of LeTID [21–23]. However, the evidence suggests that more than just hydrogen is required for the degradation to occur. Bredemeier et al. showed that phosphorus diffusion gettering which removes metal impurities from the bulk resulted in reduced levels of LeTID, leading to the hypothesis that a metal-hydrogen pair is a possible candidate for LeTID [24]. Other researchers have proposed that hydrogen is passivating point defects in the bulk of the silicon wafer and that these defects are subsequently depassivated during illumination [13,25]. Vacancy-hydrogen pairs have

* Corresponding author.
E-mail address: m.umair@unsw.edu.au (M.U. Khan).

https://doi.org/10.1016/j.solmat.2019.109990
Received 29 March 2019; Received in revised form 30 May 2019; Accepted 7 June 2019

also been proposed as a possible candidate [26]. Vacancies are a fundamental defect within a silicon lattice, however, to date they have not been the focus of any specific degradation studies on solar cells. A recent paper described an LeTID study in which vacancies were introduced during ingot growth, however that paper did not present any results that then compared between grown-in vacancies and LeTID [27]. Given their fundamental nature and ability to interact with a wide variety of lattice impurities, it is interesting to determine if vacancy related defects have similar characteristics to LeTID or if the presence of large amounts of vacancies in the lattice somehow impacts the formation or regeneration kinetics of LeTID.

Many techniques have been demonstrated that create and control the amount of vacancy defects in a silicon wafer including electron or neutron radiation [28], temperature quenching [3], and controlling the silicon growth rate [1]. In this work, we use electron radiation which has previously been used to study silicon solar cells in terms of survival in outer space applications [4,29]. It is reported that high energy electron radiation removes an atom from the lattice leaving behind a vacancy and creating a self-interstitial [6]. Neutron radiation can cause large defects such as tetra- or penta-vacancies (voids) because its high mass carries high energy [9]. However, while high energy electrons also cause the displacement of host atoms from their lattice location, the low mass of the electron results in simple damage (i.e. the creation of individual point defects) to the lattice [30]. After radiation, both vacancies and interstitials are mobile and over time either recombine with their partner or potentially interact with other impurities within the bulk [29]. Vacancies can also make pairs with other vacancies in many different charge states [31]. A high flux of electron radiation, therefore, creates more lattice defects which lead toward more defect recombination centres.

In this research, we apply a range of 1 MeV electron radiation fluences (1×10^{10} e/cm^2 to 1×10^{15} e/cm^2) to create different numbers of radiation defects in solar grade Cz p-type silicon. This is investigated in terms of LeTID and the role of hydrogen in the light and temperature stability of the radiation-induced defects in silicon solar cells. The immediate impact of the radiation is to lower the bulk lifetime and not impact the surface lifetime of the samples. The degree of degradation is related to the flux of radiation, with increased flux leading to increased defect formation. Temperature dependent lifetime spectroscopy is used to extract the Shockley-Read-Hall parameters of the dominant defect, and the results are compared to similar measurements on samples dominated by LeTID. We demonstrate that recovery in lifetime during thermal annealing occurs only in the presence of bulk hydrogen which might be vacancy passivation by hydrogen. It has previously been proposed that LeTID may be a result of vacancies or vacancy-hydrogen interactions. However, this work finds that vacancy-related defects are most likely independent of the LeTID related defect and the processes that are usually believed to pre-form and induce LeTID instead reduce the impact of radiation damage.

2. Methodology

2.1. Sample preparation

Symmetric structures for carrier lifetime testing were fabricated on 156 mm × 156 mm pseudo-square, boron doped Czochralski-grown wafers with a resistivity of 1.8 Ω cm and a thickness of 190 ± 2 μm. Saw damage was removed from the surface using a potassium hydroxide solution. This was followed by an alkaline texturing etch resulting in an upright random pyramid texture with a surface area to projection area ratio of ~1.5. After texturing, the final wafer thickness was 180 ± 3 μm. Wafers were cleaned for metallic and oxide impurities using process 1 and 2 of the radio corporation of America (RCA) technique. This process includes a 6 min dip in hydrogen peroxide (H_2O_2) and ammonium hydroxide (NH_3OH) solution followed by a 6 min submersion in a solution of hydrochloric acid (HCl) and H_2O_2. These wafers were then further submerged for a short duration in 2% hydrofluoric acid (HF) for the purpose of removing any native oxides or oxides that may have formed during the RCA process. Wafers were then placed in a phosphorus oxychloride ($POCl_3$) diffusion tube to form dual-sided n^+-emitters with a sheet resistance of 65 Ω/sq. All wafers were then cleaned again before the deposition of dielectric layers for surface passivation. A 75 nm layer of hydrogenated silicon nitride (SiN_x:H) film with 2.08 refractive index at the wavelength of 633 nm [32] was deposited on both sides at a temperature of 400 °C using a remote plasma enhanced chemical vapor deposition (r-PECVD) tool (Meyer Burger MAiA).

2.2. Processing and characterization

The wafers were split into 3 groups: (a) samples irradiated in the presence of bulk hydrogen introduced from the SiN_x:H through firing also known as hydrogenation (b) samples that were hydrogenated (i.e. fired), after the irradiation process and (c) unfired samples that were irradiated and later annealed in the absence of hydrogen. Samples were fired in an infrared in-line metallization belt-furnace (Schmid) at a setpoint temperature of 805 °C and conveyor speed of 4.5 m/min with an actual peak temperature of approximately 700 °C [33]. A process flow diagram is depicted in Fig. 1.

All three sample groups were electron radiated using a Cockcroft-Walton electron accelerator [34] with six different fluences from 1×10^{10} e/cm^2 to 1×10^{15} e/cm^2 and a fixed electron beam energy of 1 MeV [35]. The details of fluence and time are given in Table 1. Each wafer was wrapped in aluminum foil and kept on a water-cooled plate to ensure wafers remained at room temperature during irradiation. All wafers were then laser cleaved into 52 mm × 52 mm tokens for subsequent testing.

LeTID testing was carried out using the dark annealing process proposed in Refs. [36,37]. Wafer tokens were treated on a hotplate in the dark at a temperature of 150 ± 2 °C to investigate the response of vacancies to thermal treatments in the presence and absence of hydrogen. Periodic quasi-steady-state photoconductance (QSS-PC) measurements were taken during the dark annealing using the photoconductance tool (Sinton Instruments, WCT-120TS). Minority carriers recombination was analysed using the generalised method [38] and intrinsic recombination was corrected using the Richter model [39]. Effective lifetimes (τ_{eff}) were extracted at an injection level (Δn) corresponding to approximately 10% of the background boron dopant concentration [40]. Emitter saturation current density (J_{0e}) was extracted from the curves using the Kane-Swanson method [41]. Photoluminescence (PL) imaging measurements using an illumination intensity of 1 sun for 0.2 s of exposure time were taken to monitor the spatial variation of effective lifetime directly after electron irradiation.

To study the electrical parameters of the defect, temperature- and injection-dependent lifetime spectroscopy (TIDLS) measurements were done on Group (a) for samples with a fluence 1×10^{14} e/cm^2 and 1×10^{15} e/cm^2 (chosen as the samples had hydrogen in bulk). This was done using a specially designed lifetime tester which is equipped with a

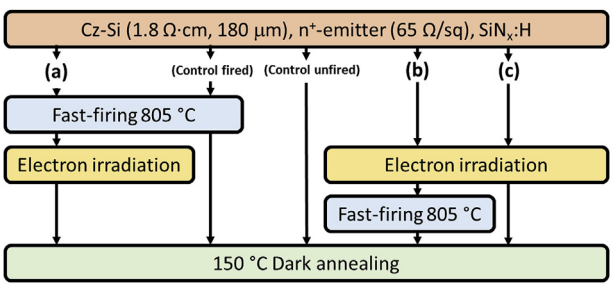

Fig. 1. Process flow diagram for investigating the impact of H on radiation-induced vacancies.

Table 1
Electron radiation of energy 1 MeV at different fluences, fluence rate and time.

Fluence (e/cm^2)	1×10^{10}	1×10^{11}	1×10^{12}	1×10^{13}	1×10^{14}	1×10^{15}
Fluence rate (e/cm^2/sec)	5.85×10^9	5.85×10^9	5.85×10^{10}	1.93×10^{11}	1.93×10^{11}	1.93×10^{11}
Time (s)	1.7	17	17	52	518	5181

temperature-controlled cryostat, photoconductance coil, and variou illumination sources [42]. After measuring injection dependent lifetime at four different setpoint temperatures, −25 °C, 0 °C, 30 °C and 50 °C, the data was corrected for intrinsic recombination [43]. The lifetime curves were then linearized using the variable change (X = n/p) method introduced by Murphy et al. [44] and fitted with one or two defects. To minimise the effects of both the bulk and the surfaces on τ_{eff}, the τ_{eff} of the irradiated samples were corrected using τ_{eff} of the reference sample,

$$\frac{1}{\tau_{SRH}} = \frac{1}{\tau_{eff}} - \frac{1}{\tau_{ref}}$$

when τ_{SRH} is the lifetime of the defect we are studying and τ_{ref} is the lifetime of the reference sample.

For each defect, the defect parameter solution surface (DPSS) measurement was used at each temperature. If we assume that the defects are independent of temperature, the defect parameters E_t and k are then determined from the intersection points of the various DPSS curves [45].

3. Results and discussion

This section starts with the impact of electron radiation on the creation of defects in silicon and the characterization of those defects with lifetime spectroscopy. Later these defects will be studied using high and low temperature processing in the presence and absence of hydrogen in bulk.

3.1. Radiation effect

This section is focused on the characterization of wafers right after electron radiation. All three groups were measured using QSS-PC techniques to measure the injection dependent lifetime. Later photoluminescence imaging was used to visualize the wafers and determine any spatial variation in recombination. Finally, the results of temperature and injection dependent lifetime spectroscopy (TIDLS) are presented for radiated wafers and the results compared to those measured on LeTID.

3.1.1. Photoluminescence and photoconductance

A summary of the effective lifetime extracted at an injection level of 8×10^{14} cm^{-3} (Table 2) reveals the clear impact of the variation in the radiation fluence on the samples. In all groups, the effective lifetime of samples was reduced with increasing irradiation fluence. Samples with the lowest fluence of 1×10^{10} e/cm^2 and 1×10^{11} e/cm^2 did not show any significant change compared to the control sample. However,

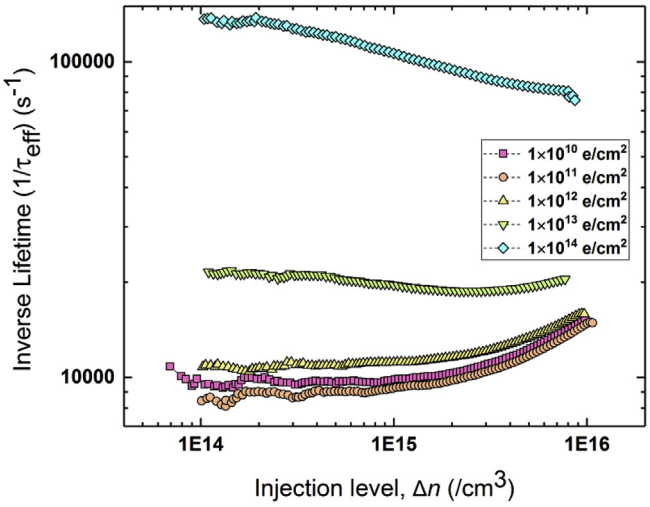

Fig. 2. Injection dependent lifetime of group (a) right after irradiation for all fluences.

1×10^{11} e/cm^2 and higher fluences showed a rapid decrease in effective lifetime. No significant impact on the emitter saturation current density was observed, although the extraction of this parameter with any confidence was only possible for the lowest three fluences since the introduction of strong bulk SRH recombination made accurate curve fitting impossible.

The Auger corrected, injection level dependent inverse lifetime curves (shown in Fig. 2 for a representative set) provide further insight into the type of recombination induced by the radiation. The reduction in effective lifetime was greatest at lower excess carrier concentrations which is consistent with the introduction of a bulk SRH defect. The impact on surface lifetime was less clear since the bulk defect makes it progressively harder to accurately extract J_{0e} from the data. In the worst case the curve is dominated by bulk recombination and no significant impact of the surface recombination on the shape of the curve remains.

Photoluminescence images of the sample taken after electron irradiation indicate that the reduction in recombination was uniform across the samples. Like the effective lifetime results, the reduction in PL intensity trended with the flux. Beyond a fluence of 1×10^{13} e/cm^2, increased radiation fluence resulted in a severe decline in the measured wafer performance (Fig. 3). Although some localized points of higher recombination were observed on the samples, these appear to have been introduced during sample preparation and are not related to the radiation damage. One interesting observation was seen in the region

Table 2
Effective minority carrier lifetime and extracted J_{0e} values after electron radiations for all groups at different fluences. Values are the average of 5 measurements and uncertainty shown was determined as the maximum and minimum value range.

		Control	Fluence (e/cm^2)					
			1×10^{10}	1×10^{11}	1×10^{12}	1×10^{13}	1×10^{14}	1×10^{15}
Group (a)	Effective Lifetime (μs)	128 ± 7	126 ± 9	110 ± 2	88 ± 5	50 ± 5	11 ± 1	1 ± 0.1
	J_{0e} (fA/cm^2)	80 ± 10	75 ± 5	76 ± 5	72 ± 4	–	–	–
Group (b) & (c)	Effective Lifetime (μs)	88 ± 5	85 ± 5	83 ± 3	74 ± 1	45 ± 2	10 ± 1	1 ± 0.1
	J_{0e} (fA/cm^2)	103 ± 8	86 ± 7	88 ± 3	78 ± 5	–	–	–

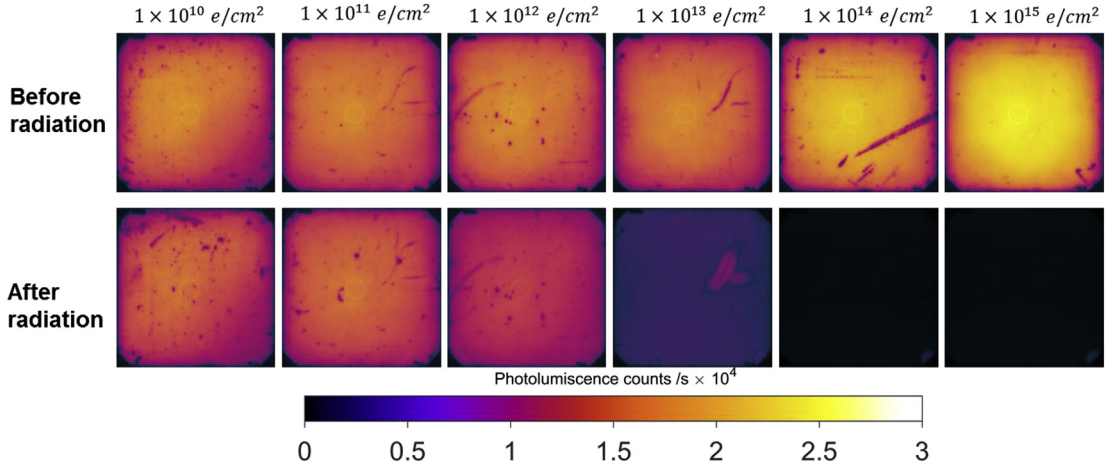

Fig. 3. PL images of samples with no firing (i.e. groups (b) and (c), bulk assumed not to have significant levels of hydrogen) before and after various fluences of electron irradiation ranging from 1×10^{10} e/cm^2 to 1×10^{15} e/cm^2.

around a surface scratch for 1×10^{13} e/cm^2 which resulted in proportionally higher PL strength. The underlying reason for this is not understood.

A similar spatial uniformity and trend in the PL intensity (and thus the effective lifetime) was seen for samples from group (a) after the electron radiation (Fig. 4). The initial PL counts of all the samples were higher in this group due to an improvement in bulk lifetime as a result of firing in the presence of a hydrogenated SiN_x:H layer.

Firing the samples prior to radiation did not impact the effective lifetime of the samples once a significant amount of damage was present. Combined with the results shown in Table 2, it can be concluded that the presence of hydrogen in the bulk during radiation did not significantly impact the lifetime of the samples measured immediately after radiation. Furthermore, it is interesting that despite the different starting effective lifetimes of the samples, the final lifetimes for the three samples with the highest radiation flux were almost the same. This indicates that the defects created by the radiation process dominate the effective lifetime of those samples.

3.1.2. Temperature and injection dependent lifetime spectroscopy (TIDLS)

Fig. 5 shows a representative example of a linearized lifetime curve of the 1×10^{14} e/cm^2 wafer after correction to τ_{ref}. The high linearity of the curve indicates that τ_{eff} of these samples is mainly affected by one defect ('dominant defect'), although, a weak impact of a second defect can be identified at low injection. The DPSS analysis is therefore done only for the dominant defect.

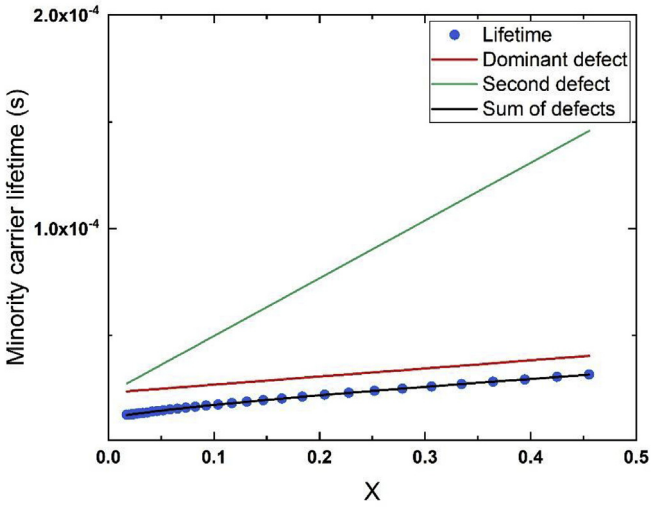

Fig. 5. Linearized lifetime curves of a representative sample for 1×10^{14} e/cm^2.

Fig. 6 shows the DPSS curves of the dominant defect for the 1×10^{14} e/cm^2 and 1×10^{15} e/cm^2, as well as the quality of the fit, that is defined as the sum of the standard deviations (STD) of all the DPSS curves from their average value for each E_t. Based on the fit

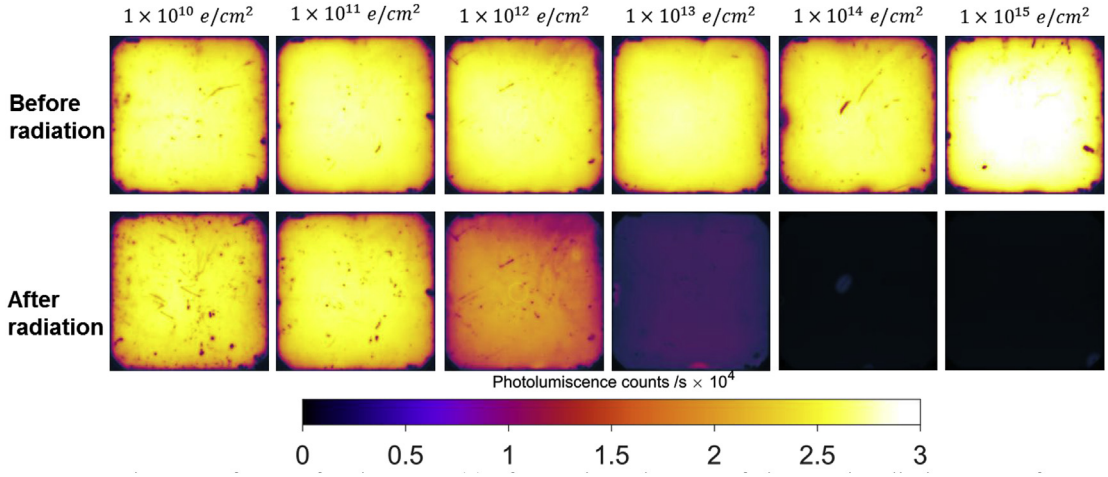

Fig. 4. PL images of Cz wafers in group (a) after various degrees of electron irradiation range from 1×10^{10} e/cm^2 to 1×10^{15} e/cm^2.

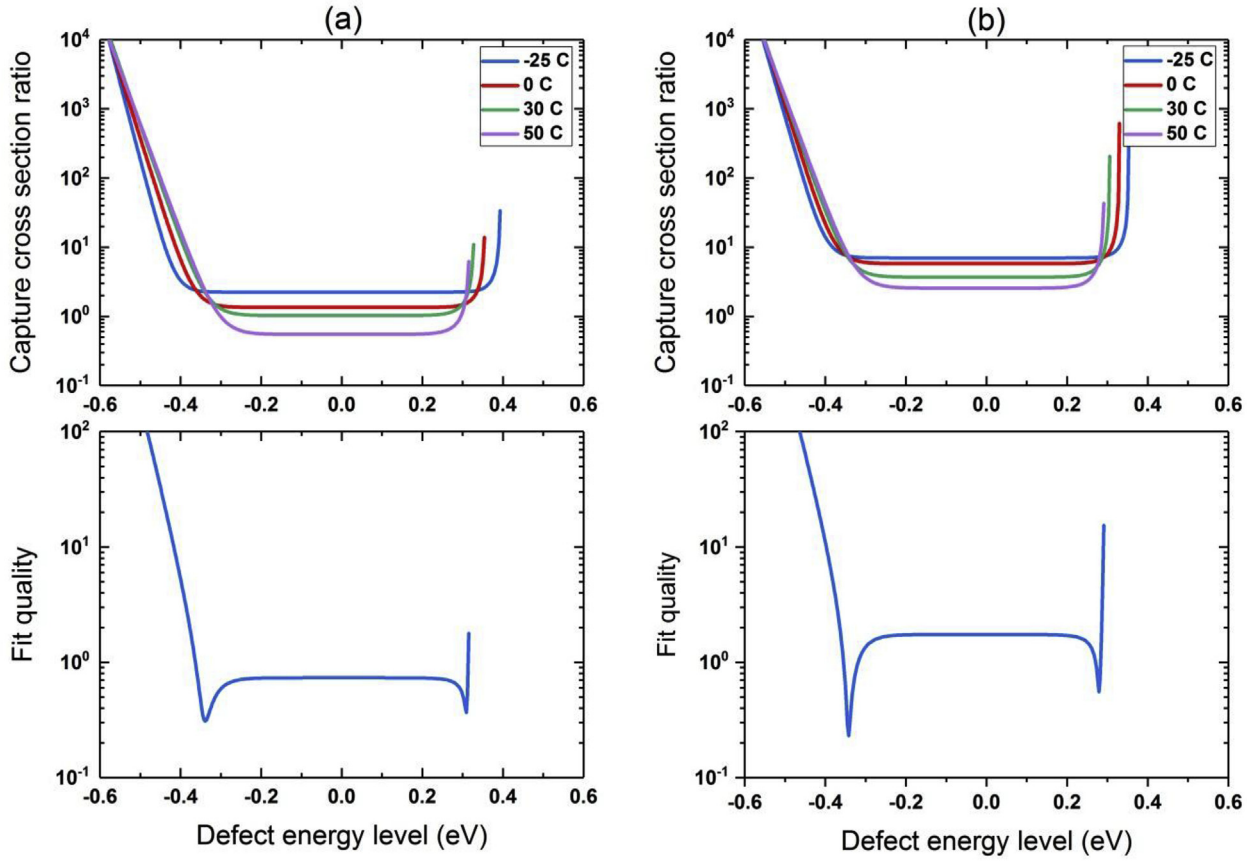

Fig. 6. DPSS-k and standard deviation of E_t - k curves of (a) 1×10^{14} e/cm^2 and (b) 1×10^{15} e/cm^2 after the electron radiation (dominant defect).

Table 3
Defect energy level and symmetry factor of the dominant defect measured using DPSS curves generated from TIDLS measurements of various samples. The uncertainty was determined based on the STD.

Sample	Defect energy level (eV)		Symmetry factor	
	Lower half	*Upper half*	*Lower half*	*Upper half*
1×10^{14} e/cm^2	−0.34 ± 0.01	0.31 ± 0.01	2.2 ± 0.3	2.0 ± 0.4
1×10^{15} e/cm^2	−0.34 ± 0.01	0.28 ± 0.01	7.3 ± 0.2	6.5 ± 0.6

quality, two possible solutions are identified, one in the lower band-gap half and one in the upper half. The extracted defect energy level E_t and the symmetry factor k are summarized in Table 3. The uncertainty range of E_t is determined based on the fit quality and represents the energy range of k ± STD.

In the lower half, a good agreement is demonstrated regarding E_t, and we can determine E_t in the range -(0.33–0.35) eV. The range of k is larger, between 1.9 and 7.5. For the upper half, the range of E_t is a bit larger 0.27–0.32 eV; nevertheless, the range of k is similar to that determined for the lower half.

Comparison of the values found in all cases above to those extracted with similar techniques on samples degraded with LeTID show little correlation. Vargas et al. [43] found the LeTID defect to have E_t-E_i = (0.19 ± 0.03) eV and k = 37 ± 8 for the upper half, and E_t-E_i = -(0.30 ± 0.03) eV and k = 39 ± 6 for the bottom half. The values measured for the SRH statistics of LeTID are therefore very different to those measured here, and as such, they are unlikely to be the same defect.

3.2. The impact of high temperature firing on radiation-induced damage

Group (b) wafers went through metallization fast firing after the electron radiation which resulted in a full recovery of carrier lifetime (see Fig. 7.). In the most extreme case, samples which received a radiation fluence of 1×10^{15} e/cm^2 were observed to recover from an effective lifetime of ~2 μs up to ~100 μs. Examination of injection level dependent lifetime curves indicates that this was due to a recovery of the bulk lifetime. This recovery could either be due to defect-annealing or passivation via hydrogen of the radiation-induced damage in the bulk. Subsequent annealing in the dark at 150 °C showed a degradation mechanism after approximately 6 h, corresponding closely with the time scales for LeTID in previous experiments [36]. The formation and eventual recovery behavior also strongly resembled that of LeTID reported in various other sources [46,47]. The control samples with the absence of radiation damage exhibited similar LeTID behavior with annealing and the presence prior to firing of radiation damage does not appear to have influenced the post-firing LeTID in any way.

Comparisons in the Shockley-Read-Hall statistics (Fig. 7b) of the defects brought about after irradiation and during subsequent annealing indicates that the defects are different. The symmetry ratio factor of the defect (k) used in this curve fitting was very similar to the value extracted using the TIDLS for the sample with a flux of 1×10^{14} e/cm^2 (corrected). These results further indicate that radiation-induced defects (which we interpret to be vacancy related) are fundamentally different from the defect formed during LeTID. Any degradation induced in the irradiated samples, in this case, can be attributed to LeTID caused by firing a sample passivated with hydrogenated silicon nitride. The presence of radiation damage prior to firing had no impact on the post-firing LeTID.

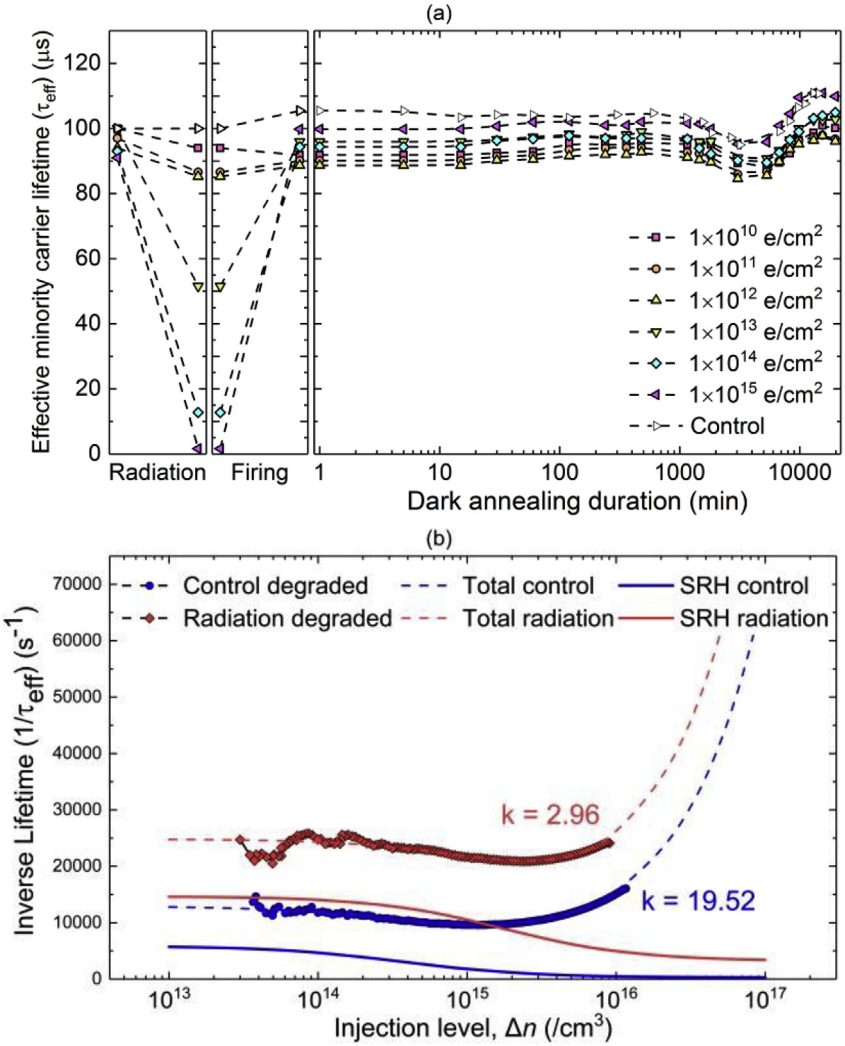

Fig. 7. (a) Effective lifetime after electron radiation, hydrogenation, and during annealing at 150 °C (b) Inverse lifetime curve at maximum degraded state of control sample, and wafer immediately after electron radiation (group (b)).

3.3. Low temperature hydrogen passivation of radiation-induced degradation

The presence of hydrogen in the bulk of the samples was found to have a significant impact on the subsequent impact of annealing on effective lifetime. Samples without firing (i.e. group (c) without any significant concentrations of bulk hydrogen) remained permanently degraded throughout annealing without any observed improvement in the effective lifetime (Fig. 8a). Wafers that had undergone a pre-hydrogenation treatment, however, instead depict a gradual recovery mechanism. Within the time scale of 2×10^4 min, almost all samples except the wafer with 1×10^{15} e/cm^2 are seen to recover entirely back to their starting lifetimes (Fig. 8b).

The recovery process of the worst affected samples shows two distinct rates. This can be attributed to the superposition of two defects changing within the bulk. Initially, the gradual improvement of the radiation damage related defect and later the formation and recovery of LeTID (like Fig. 7a). Neither the maximum extent nor the formation and recovery rates of the LeTID seem impacted by the degree of damage caused by the radiation.

It may be concluded that the recombination centres brought about through radiation damage may respond well to hydrogen or can be minimized through hydrogen passivation. A single vacancy can exist in five charge states (V^{2+}, V^{+}, V^{0}, V^{-}, V^{2-}) and all are reactive with hydrogen to make VH, VH_2, VH_3, and VH_4. These all form recombination active defects except for VH_4 which is most stable and is not recombination active [48]. The literature suggests that vacancy hydrogen complexes can induce damage in silicon [49], however in the result here hydrogen appears to improve radiation-induced damage.

4. Conclusions

This paper studied the impact of radiation induced damage on the effective lifetime of silicon wafers. It demonstrated a correlation between the fluence of radiation and the extent of Shockley-Read-Hall defects introduced into the wafer bulk. Temperature dependent lifetime spectroscopy was able to isolate the dominant defect introduced and extract its defect parameters. The thermal processes applied after the radiation did not cause any further degradation of bulk lifetime and in some cases caused a recovery. For low temperature dark annealing (150 °C) this recovery only occurred on samples that had previously been hydrogenated, demonstrating that bulk hydrogen plays a role in the recovery process. Neither the defect parameters extracted, nor the formation and recovery kinetics observed, showed any link to the LeTID process that impacts hydrogenated solar cells. Assuming the radiation induced varying amounts of vacancy and vacancy clusters into the bulk of the wafer, this study finds no evidence for any link between LeTID and vacancies in silicon.

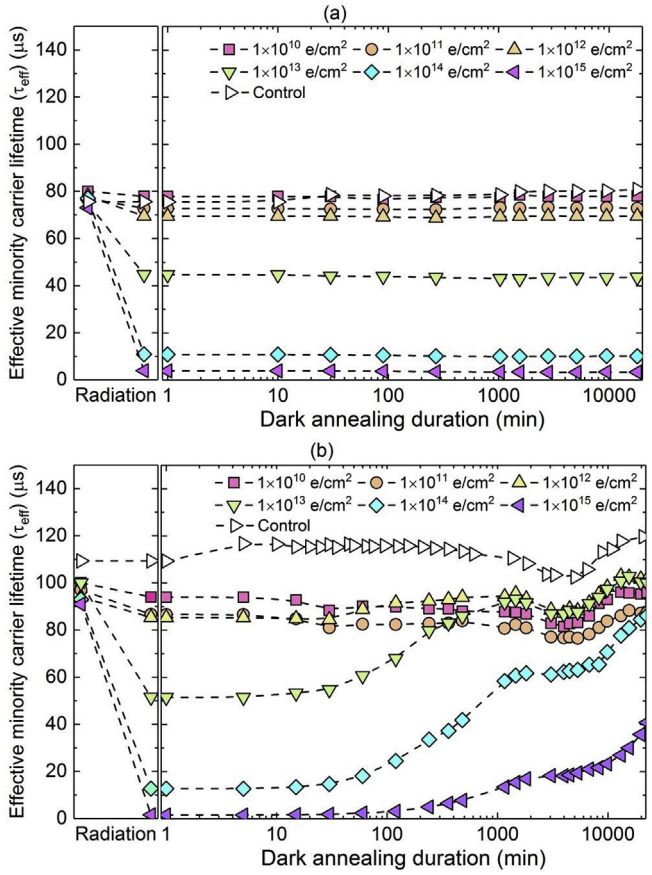

Fig. 8. Effective minority carrier lifetime as a function of DA time at a temperature of 150 °C for samples (a) without bulk hydrogenation (group (c)) and (b) with bulk introduction of hydrogen via firing (group (a)) prior to electron irradiation.

Acknowledgements

This activity received funding from ARENA as part of ARENA's Research and Development Program (ARENA 1-A060 and 2017/RND001) and the Australian Centre for Advanced Photovoltaics. The views expressed herein are not necessarily the views of the Australian Government, and the Australian Government does not accept responsibility for any information or advice contained herein.

References

[1] V.V. Voronkov, Grown-in defects in silicon produced by agglomeration of vacancies and self-interstitials, J. Cryst. Growth 310 (2008) 1307–1314, https://doi.org/10.1016/j.jcrysgro.2007.11.100.
[2] R. Søndenå, B. Ryningen, M. Juel, Minority carrier lifetimes in Cz-Si wafers with intentional V-I transitions, Energy Procedia 124 (2017) 786–793, https://doi.org/10.1016/j.egypro.2017.09.348.
[3] Y. Kraftmakher, Equilibrium vacancies and thermophysical properties of metals, Phys. Rep. 299 (1998) 79–188, https://doi.org/10.1016/S0370-1573(97)00082-3.
[4] D. Nikolić, A. Vasić-Milovanović, Comparative study of gamma and neutron irradiation effects on the silicon solar cells parameters, FME Trans. 44 (2016) 99–105, https://doi.org/10.5937/fmet1601099N.
[5] H. Bracht, J.F. Pedersen, N. Zangenberg, A.N. Larsen, E.E. Haller, G. Lulli, M. Posselt, Radiation enhanced silicon self-diffusion and the silicon vacancy at high temperatures, Phys. Rev. Lett. 91 (2003) 1–4, https://doi.org/10.1103/PhysRevLett.91.245502.
[6] G.D. Watkins, EPR of a trapped vacancy in boron doped silicon, Phys. Rev. B 13 (1976) 2511.
[7] S.B. Zhang, H.M. Branz, Hydrogen above saturation at silicon vacancies: H-pair reservoirs and metastability sites, Phys. Rev. Lett. 87 (2001) 1–4, https://doi.org/10.1103/PhysRevLett.87.105503.
[8] A.O. Evwaraye, E. Sun, Electron-irradiation-induced divacancy in lightly doped silicon, J. Appl. Phys. 47 (1976) 3776–3780, https://doi.org/10.1063/1.323260.
[9] Y.H. Lee, J.W. Corbett, EPR studies of defects in electron-irradiated silicon: a triplet state of vacancy-oxygen complexes, Phys. Rev. B 13 (1976) 2653–2666, https://doi.org/10.1103/PhysRevB.13.2653.
[10] G.D. Watkins, Intrinsic defects in silicon, Mater. Sci. Semicond. Process. 3 (2000) 227–235, https://doi.org/10.1016/S1369-8001(00)00037-8.
[11] M. Xiajie, The complexity of LID, LeTID and HID, (n.d.). https://www.pv-tech.org/white-papers/the-complexity-of-lid-letid-and-hid.
[12] M. Wagner, F. Wolny, M. Hentsche, A. Krause, L. Sylla, F. Kropfgans, M. Ernst, R. Zierer, P. Bönisch, P. Müller, N. Schmidt, V. Osinniy, H.-P. Hartmann, R. Mehnert, H. Neuhaus, Correlation of the LeTID amplitude to the Aluminium bulk concentration and Oxygen precipitation in PERC solar cells, Sol. Energy Mater. Sol. Cells 187 (2018) 176–188, https://doi.org/10.1016/j.solmat.2018.06.009.
[13] D. Chen, P.G. Hamer, M. Kim, T.H. Fung, G. Bourret-Sicotte, S. Liu, C.E. Chan, A. Ciesla, R. Chen, M.D. Abbott, B.J. Hallam, S.R. Wenham, Hydrogen induced degradation: a possible mechanism for light- and elevated temperature- induced degradation in n-type silicon, Sol. Energy Mater. Sol. Cells 185 (2018) 174–182, https://doi.org/10.1016/j.solmat.2018.05.034.
[14] I.L. Kolevatov, P.M. Weiser, E.V. Monakhov, B.G. Svensson, Interaction between hydrogen and vacancy defects in crystalline silicon, Phys. Status Solidi Appl. Mater. Sci. 1800670 (2018) 1–10, https://doi.org/10.1002/pssa.201800670.
[15] A. Ramspeck, K., S. Zimmermann, H. Nagel, A. Metz, Y. Gassenbauer, B. Birkmann, Seidl, Light induced degradation of rear passivated mc-Si solar cells, 27th Eur. Photovolt. Sol. Energy Conf. 2012, pp. 861–865, , https://doi.org/10.1017/CBO9781107415324.004.
[16] A. Herguth, C. Derricks, P. Keller, B. Terheiden, Recovery of LeTID by low intensity illumination: reaction kinetics, completeness and threshold temperature, Energy Procedia 124 (2017) 740–744, https://doi.org/10.1016/j.egypro.2017.09.090.
[17] M.A. Jensen, A.E. Morishige, S. Chakraborty, R. Sharma, H.C. Sio, C. Sun, B. Lai, V. Rose, A. Youssef, E.E. Looney, S. Wieghold, D. Macdonald, J.B. Li, T. Buonassisi, Do grain boundaries matter ? Electrical and elemental identification at grain boundaries in LeTID-affected p -type multicrystalline silicon, IEEE-PVSC. (2017) 6–9.
[18] D. Macdonald, F. Rougieux, A. Cuevas, B. Lim, J. Schmidt, M. Di Sabatino, L.J. Geerligs, Light-induced boron-oxygen defect generation in compensated p -type Czochralski silicon, J. Appl. Phys. 105 (2009), https://doi.org/10.1063/1.3121208.
[19] J.M. Fritz, A. Zuschlag, D. Skorka, A. Schmid, G. Hahn, Temperature dependent degradation and regeneration of differently doped mc-Si materials, Energy Procedia 124 (2017) 718–725, https://doi.org/10.1016/j.egypro.2017.09.085.
[20] H.C. Sio, H. Wang, Q. Wang, C. Sun, W. Chen, H. Jin, D. Macdonald, Light and elevated temperature induced degradation in p-type and n-type cast-grown multicrystalline and mono-like silicon, Sol. Energy Mater. Sol. Cells 182 (2018) 98–104, https://doi.org/10.1016/j.solmat.2018.03.002.
[21] J. Mullins, V.P. Markevich, M.P. Halsall, A.R. Peaker, Evidence for molybdenum-hydrogen bonding in p-type silicon upon annealing under illumination, Phys. Status Solidi 1800611 (2018) 1–7, https://doi.org/10.1002/pssa.201800611.
[22] L. Song, J. Lou, J. Fu, Z. Ji, Impact of various charge states of hydrogen on passivation of dislocation in silicon, Electron. Mater. Lett. 14 (2018) 574–580, https://doi.org/10.1007/s13391-018-0061-y.
[23] A. Ciesla, S. Wenham, R. Chen, C. Chan, D. Chen, B. Hallam, D. Payne, T. Fung, M. Kim, S. Liu, S. Wang, K. Kim, A. Samadi, C. Sen, C. Vargas, U. Varshney, B.V. Stefani, P. Hamer, N. Nampalli, Z. Hameiri, C. Chong, M. Abbott, Hydrogen-induced degradation, EEE 7th World Conference on Photovoltaic Energy Conversion (WCPEC), 2018, pp. 0001–0008, , https://doi.org/10.1109/PVSC.2018.8548100.
[24] D. Bredemeier, D. Walter, S. Herlufsen, J. Schmidt, Understanding the light-induced lifetime degradation and regeneration in multicrystalline silicon, Energy Procedia 92 (2016) 773–778, https://doi.org/10.1016/j.egypro.2016.07.060.
[25] K. Nakayashiki, J. Hofstetter, A.E. Morishige, T.T.A. Li, D.B. Needleman, M.A. Jensen, T. Buonassisi, Engineering solutions and root-cause analysis for light-induced degradation in p-type multicrystalline silicon PERC modules, IEEE J. Photovoltaics. 6 (2016) 860–868, https://doi.org/10.1109/JPHOTOV.2016.2556981.
[26] T.H. Fung, M. Kim, D. Chen, C.E. Chan, B.J. Hallam, R. Chen, D.N.R. Payne, A. Ciesla, S.R. Wenham, M.D. Abbott, A four-state kinetic model for the carrier-induced degradation in multicrystalline silicon: introducing the reservoir state, Sol. Energy Mater. Sol. Cells 184 (2018) 48–56, https://doi.org/10.1016/j.solmat.2018.04.024.
[27] M. Wagner, F. Wolny, M. Hentsche, A. Krause, L. Sylla, F. Kropfgans, M. Ernst, R. Zierer, P. Bönisch, P. Müller, N. Schmidt, V. Osinniy, H.-P. Hartmann, R. Mehnert, H. Neuhaus, Correlation of the LeTID amplitude to the Aluminium bulk concentration and Oxygen precipitation in PERC solar cells, Sol. Energy Mater. Sol. Cells 187 (2018) 176–188, https://doi.org/10.1016/j.solmat.2018.06.009.
[28] B. Simit, D. Nikolit, K. Stankovit, L. Timotijevit, S. Stankovit, Damage induced by neutron radiation on output characteristics of solar cells, photodiodes, and photo-transistors, Int. J. Photoenergy 2013 (2013), https://doi.org/10.1155/2013/582819.
[29] A. Khan, M. Yamaguchi, Y. Ohshita, N. Dharmarasu, K. Araki, T. Abe, H. Itoh, T. Ohshima, M. Imaizumi, S. Matsuda, Role of the impurities in production rates of radiation-induced defects in silicon materials and solar cells, J. Appl. Phys. 90 (2001) 1170–1178, https://doi.org/10.1063/1.1384855.
[30] P. Song, J. Liu, H. Xu, Y. Wang, Quantitative analysis of the degradation behavior of silicon solar cell irradiated by 1 MeV electron beams using photocarrier radiometry combined with lock-in carrierography, Int. J. Thermophys. 39 (2018) 128, https://doi.org/10.1007/s10765-018-2445-5.
[31] A.H.M. Smets, C.R. Wronski, M. Zeman, M. van de Sanden, The staebler-wronski effect: new physical approaches and insights as a route to reveal its origin, MRS Proc. 1245 (2010), https://doi.org/10.1557/PROC-1245-A14-02 1245-A14-02.

[32] Z. Hameiri, N. Borojevic, L. Mai, N. Nandakumar, K. Kim, S. Winderbaum, Should the refractive index at 633 nm be used to characterize silicon nitride films? IEEE 43rd Photovolt. Spec. Conf. IEEE, 2016, pp. 2900–2904, , https://doi.org/10.1109/PVSC.2016.7750187 2016.

[33] D. Chen, M. Kim, B.V. Stefani, B.J. Hallam, M.D. Abbott, C.E. Chan, R. Chen, D.N.R. Payne, N. Nampalli, A. Ciesla, T.H. Fung, K. Kim, S.R. Wenham, Evidence of an identical firing-activated carrier-induced defect in monocrystalline and multi-crystalline silicon, Sol. Energy Mater. Sol. Cells 172 (2017) 293–300, https://doi.org/10.1016/j.solmat.2017.08.003.

[34] National Institutes for Quantum and Radiological Science and Technolog, Electron beam irradiation facility, (n.d.). https://www.taka.qst.go.jp/tiara/665/english/Acc_index.php.

[35] Takao K. Kanazawa, Yasuyuki Haruyama, Sadanori Uno, Keiichi Yotsumoto, Ryuichi Tanaka, Masamitsu Washino, Yoshida, Output Characteristics of 2 MeV, 60 kW, Dual Beam Type Electron Accelerator of TRCRE, JAERI, 1986.

[36] D. Chen, M. Kim, B.V. Stefani, B.J. Hallam, M.D. Abbott, C.E. Chan, R. Chen, D.N.R. Payne, N. Nampalli, A. Ciesla, T.H. Fung, K. Kim, S.R. Wenham, Evidence of an identical firing-activated carrier-induced defect in monocrystalline and multi-crystalline silicon, Sol. Energy Mater. Sol. Cells 172 (2017) 293–300, https://doi.org/10.1016/j.solmat.2017.08.003.

[37] C. Chan, T.H. Fung, M. Abbott, D. Payne, A. Wenham, B. Hallam, R. Chen, S. Wenham, Modulation of carrier-induced defect kinetics in multi-crystalline silicon PERC cells through dark annealing, Sol. RRL. 1 (2017) 1600028, https://doi.org/10.1002/solr.201600028.

[38] H. Nagel, C. Berge, A.G. Aberle, H. Nagel, C. Berge, A.G. Aberle, Generalized analysis of quasi-steady-state and quasi-transient measurements of carrier lifetimes in semiconductors Generalized analysis of quasi-steady-state and quasi-transient measurements of carrier lifetimes in semiconductors, J. Appl. Phys. 86 (1999) 6218–6221, https://doi.org/10.1063/1.371633.

[39] A. Richter, F. Werner, A. Cuevas, J. Schmidt, S.W. Glunz, Improved parameterization of auger recombination in silicon, Energy Procedia 27 (2012) 88–94, https://doi.org/10.1016/j.egypro.2012.07.034.

[40] T.U. Naerland, H. Haug, H. Angelskar, R. Sondena, E.S. Marstein, L. Arnberg, Studying light-induced degradation by lifetime decay analysis: excellent fit to solution of simple second-order rate equation, IEEE J. Photovoltaics 3 (2013) 1265–1270, https://doi.org/10.1109/JPHOTOV.2013.2278663.

[41] K.D. E, S.R. M, Measurement of the emitter saturation current by a contactless photoconductivity decay method, 18th IEEE Photovolt. Spec. Conf. 1985, pp. 578–581.

[42] J. Schmidt, R.A. Sinton, DEFECT CHARACTERIZATION BY TEMPERATURE AND INJECTION-DEPENDENT LIFETIME SPECTROSCOPY, Process Device Model. Integr. Circuit Des. 3rd World Conference on Photovoltaic Energy Conversion, 2003, pp. 947–950.

[43] C. Vargas, Y. Zhu, G. Coletti, C. Chan, D. Payne, M. Jensen, Z. Hameiri, Recombination parameters of lifetime-limiting carrier-induced defects in multi-crystalline silicon for solar cells, Appl. Phys. Lett. 110 (2017), https://doi.org/10.1063/1.4977906.

[44] J.D. Murphy, K. Bothe, R. Krain, V.V. Voronkov, R.J. Falster, Parameterisation of injection-dependent lifetime measurements in semiconductors in terms of Shockley-Read-Hall statistics: an application to oxide precipitates in silicon, J. Appl. Phys. 111 (2012), https://doi.org/10.1063/1.4725475.

[45] S. Rein, Lifetime Spectroscopy: A Method of Defect Characterization in Silicon for Photovoltaic Applications, (2005).

[46] M.A. Jensen, A.E. Morishige, J. Hofstetter, D.B. Needleman, T. Buonassisi, Evolution of LeTID defects in p-type multicrystalline silicon during degradation and regeneration, IEEE J. Photovoltaics 7 (2017) 980–987, https://doi.org/10.1109/JPHOTOV.2017.2695496.

[47] C. Chan, T.H. Fung, M. Abbott, D. Payne, A. Wenham, B. Hallam, R. Chen, S. Wenham, Modulation of carrier-induced defect kinetics in multi-crystalline silicon PERC cells through dark annealing, Sol. RRL. 1 (2017) 1600028, https://doi.org/10.1002/solr.201600028.

[48] S.A. Centoni, B. Sadigh, G.H. Gilmer, T.J. Lenosky, T. Díaz De La Rubia, C.B. Musgrave, First-principles calculation of intrinsic defect formation volumes in silicon, Phys. Rev. B Condens. Matter 72 (2005) 1–9, https://doi.org/10.1103/PhysRevB.72.195206.

[49] H. Hatakeyama, M. Suezawa, V.P. Markevich, K. Sumino, formation of hydrogen-oxygen-vacancy complexes in silicon, Mater. Sci. Forum 196–201 (1995) 939–944 https://doi.org/10.4028/www.scientific.net/MSF.196-201.939.